Sensors and Materials, Vol. 18, No. 6 (2006) 301–312
MYU Tokyo

S & M 0651

Design Optimization of SAW Pressure Sensor with Equivalent Circuit Model

Wen Wang, Keekeun Lee*, Sangsik Yang and Ikmo Park

Division of Electronics Engineering, Ajou University, Suwon 443-749, Korea

(Received December 12, 2005; accepted May 18, 2006)

Key words: equivalent circuit model, finite element method, pressure sensor, reflective delay line, surface acoustic wave

In this paper, we present a novel surface acoustic wave (SAW)-based pressure sensor, which is composed of a broadband reflective delay line and a bonding substrate with a ~250 μm deep cavity. Using the equivalent circuit model, the SAW device was simulated, and the effects of interdigital transducer (IDT) structure, acoustic aperture size, and the number of IDT finger pairs on the device performance were studied. The finite element method (FEM) was used to calculate the diaphragm bending and the resultant stress/strain distribution along the diaphragm. From the simulated results, the optimal design parameters were determined. A new 440 MHz SAW pressure sensor on a 41°YX $LiNbO_3$ substrate was developed. The measured reflection coefficient S_{11} showed a high S/N ratio, a sharp reflected peak, and a large dynamic separation between the reflected peaks. The measured results matched well with the simulated results. When a mechanical compression force was applied to the diaphragm, the diaphragm was bent, resulting in time and phase angle shifts of the reflected peaks. The phase shifts were modulated depending on the amount of applied pressure. The sensitivity obtained was 2.6°/kPa.

1. Introduction

In recent years, wireless passive surface acoustic wave (SAW) pressure sensors have attracted increasing attention in consumer electronics and communication systems, because (1) they do not require any battery for activation, (2) they can be placed in hazardous environments such as contaminated and high-voltage areas, and can be accessed wirelessly, and (3) they are small, light, and can withstand even extremely harsh environmental conditions.[1–5] Several groups have reported successful SAW pressure sensors, especially for tire pressure monitoring system (TPMS) applications.[6,7] However, despite some reported success stories, current SAW pressure sensors suffer from large signal attenuation, broad reflection peaks, large noise or interference peaks, and signal evaluation errors.

For human recognition on an intelligent building floor, we fabricated a new SAW-based pressure sensor on a 41°$LiNbO_3$ substrate. Figure 1 shows a simple schematic of the

*Corresponding author, e-mail address: keekeun@ajou.ac.kr

SAW pressure sensor. It is composed of a broadband reflective delay line and a bonding substrate with a ~250 μm deep cavity. A RF pulse is transmitted from the network analyzer to a SAW transponder through the contact pads of the SAW sensor. An interdigital transducer (IDT), which is connected to the contact pads, transforms the received RF signal into a SAW. Three reflectors are placed in a row on the propagation path of the SAW. The propagating SAW partially reflects from the reflectors. The reflected SAW is reconverted into electromagnetic waves by the IDT and transmitted to the measurement unit. A pressure difference induces the bending of the diaphragm. The bending changes the SAW propagation length and velocity, resulting in phase shifts of the reflected peaks. By evaluating the phase shifts, we can extract the pressure values.

On the basis of the equivalent circuit model, the SAW reflective delay line was simulated prior to fabrication and then the optimal design parameters were determined. The primary goals were to obtain a high S/N ratio, a small signal attenuation, a sharp reflection peak, and a clear separation between reflected peaks. Using finite element methods (FEMs), the diaphragm bending and the stress/strain distribution along the diaphragm were calculated. According to the design parameters determined, a new SAW-based pressure sensor operating at 440 MHz was fabricated and characterized.

2. Analysis Modeling and Computer Simulation

2.1 *Equivalent circuit model*

The equivalent circuit model was used to predict device performance prior to fabrication. It is based on the crossed-field Mason circuit, which was originally developed to describe the launching and detection of bulk acoustic wave devices.[8] In this model, the SAW IDT is represented by a three-port network, two acoustic ports and an electric port, as shown in Fig. 2(a).[9,10] Furthermore, the SAW IDT and equivalent motional acoustic waves can be described using the admittance matrix Y, and transformed to lumped circuit elements composed of resistors, inductors, and capacitors. Since discrete elements are used, this method is also called lumped element modeling. Figure 2(b) shows the equivalent circuit of the SAW reflective delay line with three reflectors.

The Y matrix representation of this configuration can be written as

$$Y = \begin{bmatrix} y_{11} & y_{12} \\ y_{21} & y_{22} \end{bmatrix},$$

where

$$y_{11}=G_a+j(B_a+wC_1)$$

.

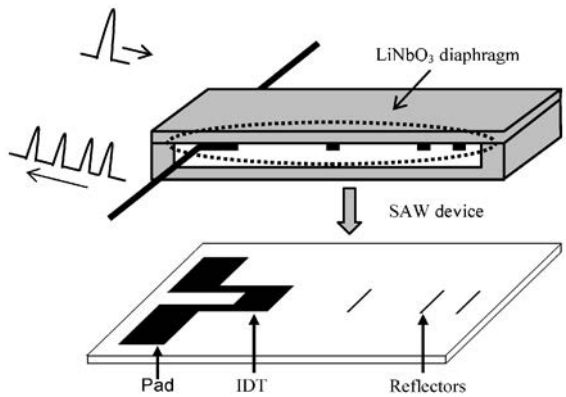

Fig. 1. Schematic of SAW-based pressure sensor.

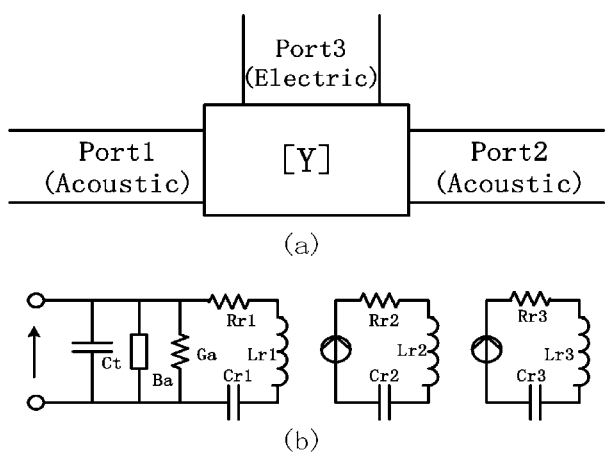

Fig. 2. Equivalent circuit model of SAW devices. (a) Three-port equivalent admittance (*Y*) network of IDT, and (b) equivalent circuit for IDT and three reflectors.

$$y_{12} = \sqrt{G_a /(R_{r1} + j\omega L_{r1} + 1/ j\omega C_{r1})(R_{r2} + j\omega L_{r2} + 1/ j\omega C_{r2})}$$
$$\times\sqrt{1/(R_{r3} + j\omega L_{r3} + 1/ j\omega C_{r3})}e^{\frac{-j\omega(M_1+M_2+M_3)}{f_0}}$$

$$y_{21}=y_{12}$$

$$y_{22}=1/(R_{r3}+j\omega L_{r3}+1/j\omega C_{r3}). \quad (1)$$

Here, the radiation conductance $G_a=g_a(\sin x/x)$, where $g_a=4/\pi K^2\omega_0 C_s W\frac{v_s}{f_0}N^2$ and $x=N\pi\left(\frac{\omega-\omega_0}{\omega_0}\right)$. The radiation susceptance $B_a=b_a\left(\frac{\sin 2x-2x}{2x^2}\right)$. C_t $(=NC_sWv_s/f_0)$ is the total static capacitance of the IDT, and C_s is the static capacitance of one periodic section. K^2 is the electromechanical coupling coefficient, ω_0 is the synchronous angular frequency, N is the number of periodic sections of the IDT, M_1 is the center distance between the IDT and the first reflector, M_2 is the center distance between the first and second reflectors, and M_3 is the center distance between the second and third reflectors. v_s is the velocity of the SAW and W is the acoustic aperture. In addition, elements L_{ri}, R_{ri}, and C_{ri} (i=1,2,3) represent equivalent motional parameters under the series resonance condition, and i stands for the reflection by the i^{th} reflector.

Using the admittance matrix Y, the reflection coefficient S_{11} of the SAW device can be determined by

$$S_{11}=\frac{(Y_G-y_{11})\times(Y_G+y_{22})+y_{12}\times y_{21}}{(Y_G+y_{11})\times(Y_G+y_{22})-y_{12}\times y_{21}}, \quad (2)$$

where Y_G is the resource and load inductance.[11]

2.2 *Equivalent circuit model simulation*

A 440 MHz SAW reflective delay line with three reflectors was simulated using the equivalent circuit model. The design parameters used for the simulation are shown in Table 1. 41° YX $LiNbO_3$ was used as a piezoelectric substrate because it has a high SAW propagation velocity (free surface: 4792.2 m/s; metal surface: 4379.7 m/s) and a large electromechanical coupling factor K^2 (17.2%).[12] The effects of the number of IDT finger pairs, acoustic aperture size, and reflector shape on the device characteristics were simulated (Table 1). Group 1 compares the device properties of two reflective delay lines with different numbers of IDT finger pairs. Decreasing the number of IDT finger pairs improves the S/N ratio and sharpens he reflecton peaks, because larger finger pairs induce

Table 1
Effects of design parameters on SAW device characteristics.

		Group 1		Group 2	
Device Parameters	IDT pair number	10	50	10	10
	Aperture	50λ	50λ	50λ	100λ
	Reflector type	Bar	Bar	Bar	Bar
	Electrode material	Al	Al	Al	Al
Simulation results for 1st reflector peak	Loss (dB)	35	44	35	34
	Bandwidth/70dB (μs)	0.09	0.16	0.089	0.083
	Dynamic separation (dB)	40	38	40	31

a stronger SAW radiation force but, at the same time, the loss is also increased by the increases in self-reflections and the circuit factor (static IDT capacitance). Group 2 compares two reflective delay lines with different apertures, where the number of IDT finger pairs was fixed at 10. The change in acoustic aperture affects only the dynamic separation of the reflected peaks in the time domain. As the acoustic aperture was increased, the dynamic separation decreased.

Figure 3 shows the reflection coefficients S_{11} in the time domain obtained from different reflector shapes (bar-type and IDT-type reflectors). It shows that a bar-type reflector effectively reduces the spurious peaks caused by a multireflection, compared with the IDT-type reflector, because the IDT-type reflector increases the self-reflection in the reflectors. From these results, we suggest that the selection of a larger acoustic aperture and a smaller IDT pair number, and the use of a bar-type reflector are effective in improving the performance of the SAW sensor.

2.3 *Finite element method (FEM)*

A FEM was used to analysis the diaphragm under an applied mechanical compression force. The bending of the diaphragm and the resultant stress/strain distribution along the diaphragm at a given pressure were calculated. The dimension of the $LiNbO_3$ diaphragm (Young's modulus: 119 GPa) used was 8 mm length × 4 mm width × 350 μm thickness.[13] The diaphragm was divided into finite small units. The diaphragm was fixed at the edges and a pressure of 300 kPa was applied to the center of the diaphragm. Figure 4 shows the calculated bending of the diaphragm and the strain distribution along the SAW propagation direction at a pressure of 300 kPa. There are compressed and stretched sections along the bent diaphragm. The stretched section was observed near the center of the diaphragm, whereas the compressed strain section was observed near the edge of the diaphragm. It is known that the SAW propagation velocity is lower in the stretched section and higher in the

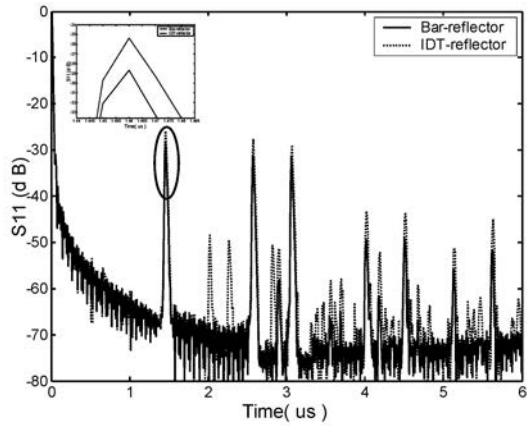

Fig. 3. Simulated S_{11} values obtained from two reflective delay lines with different types of reflector: bar-type and IDT-type reflectors.

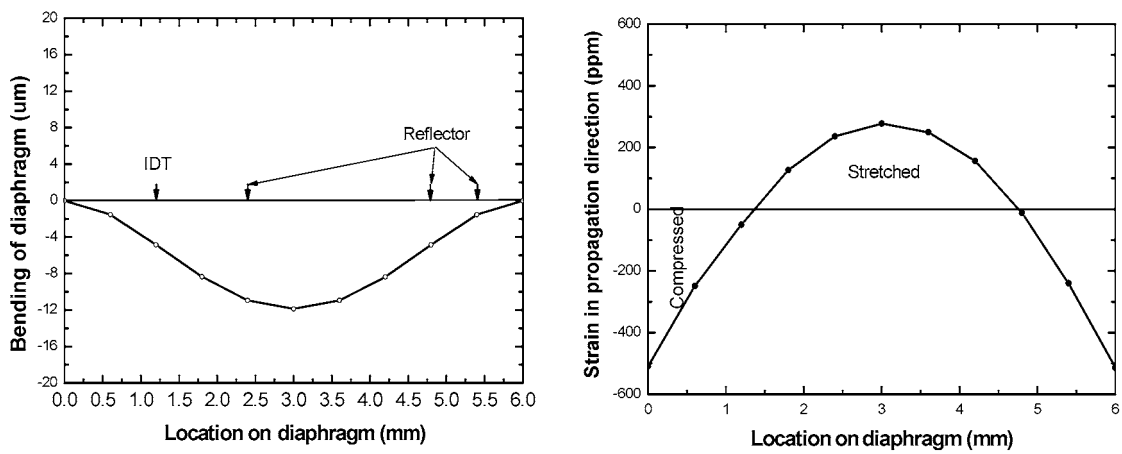

(a) (b)

Fig. 4. (a) Calculated bending of diaphragm at 300 kPa pressure and (b) strain distribution due to bending along SAW propagation direction.

compressed section. According to the obtained simulation results, to avoid a large temperature-dependent effect, the first and second reflectors should be placed in a stretched position, and the third reflector should be placed in a compressed position.

3. Evaluations of Sensitivity

A pressure difference results in the bending of the diaphragm and a stress/strain displacement along the diaphragm (Fig. 4). These cause changes in the propagation length and velocity of the SAW, which lead to time and phase angle shifts in the reflected peaks.[14] The change in the SAW propagation length, ΔL, is determined by the bending of the diaphragm, whereas the velocity shift Δv_s is decided by the stress/strain distribution on the diaphragm. The differential time delay $\Delta\tau$ for each reflector can be extracted using

$$\Delta\tau/\tau=\Delta L/L-\Delta v_s/ v_s. \tag{3}$$

Then, the phase shift $\Delta\Phi$ for each reflection peak is derived from

$$\Delta\Phi=2\pi f_0\times\Delta\tau, \tag{4}$$

where f_0 is the center frequency. Under a given pressure, the bending of the diaphragm induces approximately subnanosecond (~ns) time shifts in the reflected peaks. It is difficult to find an applied pressure value using a ~ns time shift, so we used the phase angle shift (of several degrees) to evaluate the pressure value.

The total combined phase information $\Delta\Phi_s$ for the three reflectors can be obtained from

$$\Delta\Phi_s=\Phi_2-\Phi_1-w(\Phi_3-\Phi_2). \tag{5}$$

Φ_1, Φ_2, and Φ_3 are the phase angles from each of the reflectors, and w is the ratio of the first-to-second reflector distance to the second-to-third reflector distance. As w is increased, the temperature effect can be minimized.[15]

4. Technical Realization

Using the simulation results described above, a new 440 MHz SAW reflective delay line with three reflectors was fabricated. The details of the design parameters used are shown in Table 2. Three reflectors were arranged along the SAW propagation direction in a row. The distance between the IDT and the first reflector was set at 310λ (~3084 μm), and the distance between the first and second reflectors was set at 260λ (~2590 μm).

Schematic of the fabrication procedures are shown in Fig. 5. A 4" 41°YX $LiNbO_3$ piezoelectric substrate of 350 μm thickness was used owing to its high SAW velocity and large K^2. The substrate was cleaned in acetone and rinsed in deionized (DI) water (Fig. 5(a)). A ~1500-Å-thick aluminum layer was deposited on the piezoelectric substrate using an electron beam evaporator (Fig. 5(b)). Then, a ~1-μm-thick photoresist (PR) layer was

Table 2
Design parameters of fabricated SAW-based pressure sensor.

Design Parameters		Design parameters	
Cent. frequency (MHz)	440	Acoustic aperture	50λ
IDT pair number	20	Electrode material	Al
Reflector number	3	Diaphragm dimension (Length, Width, Thickness (8 mm, 4 mm, 350 μm))	
Reflector type	Bar	Substrate material	41°YX-$LiNbO_3$

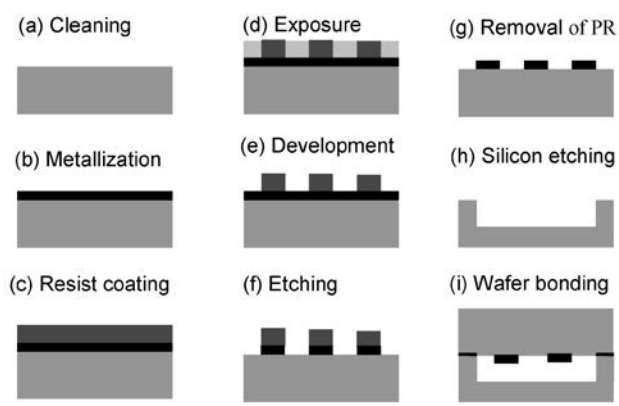

Fig. 5. Fabrication procedure for SAW pressure sensor: (a) wafer cleaning, (b) metallization, (c) photoresist (PR) spinning, (d) exposure, (e) development, (f) etching, (g) removal of PR, (h) heavily doped silicon etching and ground shielding with gold, and (i) wafer bonding with epoxy.

spin-coated, exposed, and then patterned for the IDT and three reflectors. SAW piezoelectric substrates are anisotropic. Their SAW propagation characteristics are not constant in all directions. The proper alignment of the IDT pattern with the required X-direction (X-axis wave propagation) was accomplished during the PR lithography process. Aluminum was wet-etched in 4 H_3PO_4 : 1 HNO_3 : 4 CH_3COOH : 1 H_2O etchant (Fig. 5(f)). The PR was dissolved in acetone (Fig. 5(g)). The substrate was dicing-sawed for wafer bonding and packaging. To bend the diaphragm under a pressure, a cavity ~200 μm deep on a heavily doped silicon substrate was fabricated in tetramethyl ammonium hydroxide (TMAH) solution using a SiO_2 masking layer (Fig. 5(h)). A heavily doped Si substrate provides a low resistivity like a metal, resulting in good ground shielding during network analyzer measurements. Gold was deposited all over a silicon substrate by sputtering. The diaphragm was then attached to the silicon bonding substrate with an epoxy (Fig. 5(i)).

Figure 6 shows optical microscopy and scanning electron microscopy (SEM) images of the fabricated devices. The number of IDT finger pairs was 20, the width was ~2.5 μm, the aluminum thickness was 0.1 μm, and the overlapping aperture was ~500 μm (50λ). Three reflectors were arranged in a row. The ratio of the distance between the first and second reflectors to the distance between the second and third reflectors was 3.5 to minimize the temperature dependence effect. The diaphragm was well aligned with the bottom silicon substrate, as shown in Fig. 6(b). Wire-soldering was performed to complete the electrical connection between the SAW sensor and the coaxial cable.

5. Results

The reflection coefficient S_{11} of the SAW device in the time domain was measured using an HP 8510 network analyzer and a cascade probe station. The frequency was swept from 400 to 450 MHz. Three clear peaks were observed from three reflectors (Fig. 7). A large S/N ratio, sharp peaks, and a large dynamic separation between the peaks were observed. The first reflection occurred at 1.3 μs, and at that point S_{11} was ~35 dB. The measured result (solid line) shows a good agreement with the simulation one (dotted line). The rest of the small peaks are considered to be from multiple reflections between periodically spaced reflectors (Fig. 8). For these promising results, we conclude that (1) the equivalent circuit approach is a good selection for the simulation of the sensor, (2) all the device parameters had good impedance matching with the propagating SAW, and (3) good ground shielding was obtained all over the bottom silicon substrate, which protects the fabricated device from random variations such as noise, temperature, and other environment factors during testing.

A mechanical compression force ranging from 0 to 400 kPa was applied to the diaphragm of the sensor. Figure 9 shows the phase shifts of the sensor as a function of applied compression force. There is a good linearity between phase shift and pressure in the pressure range of 0 to 300 kPa. The sensitivity was evaluated to be about 2.6°/kPa. This value is better than other reported values for similar devices. Scherr et al. reported about 2.38°/kPa in sensitivity and a linear region up to 250 kPa.[15]

The temperature-dependent effect of the fabricated sensor was tested on a hot plate. Figure 9 also shows the temperature dependence of the phase shifts depending on applied mechanical force. Stable temperature insensitivity was observed from 20 to 80°C. No

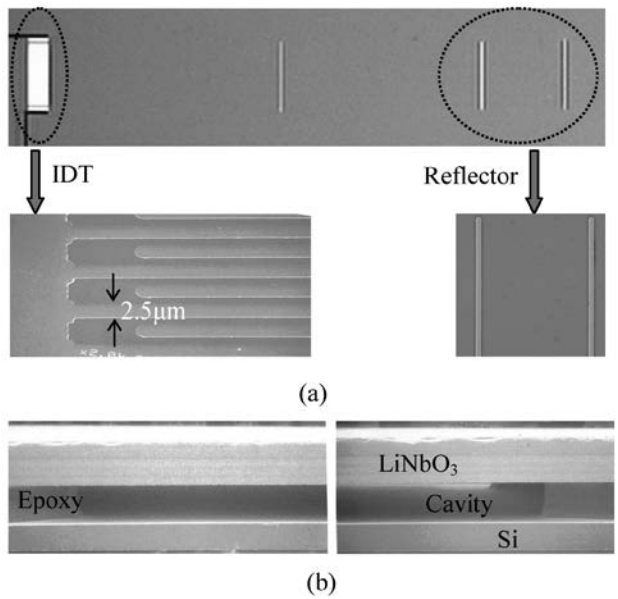

Fig. 6. Optical microscopy and scanning electron microscopy (SEM) images of fabricated SAW pressure sensor. (a) Entire view of fabricated device and magnified views of IDT-type and bar-type reflectors, and (b) wafer bonding between diaphragm and silicon substrate with epoxy.

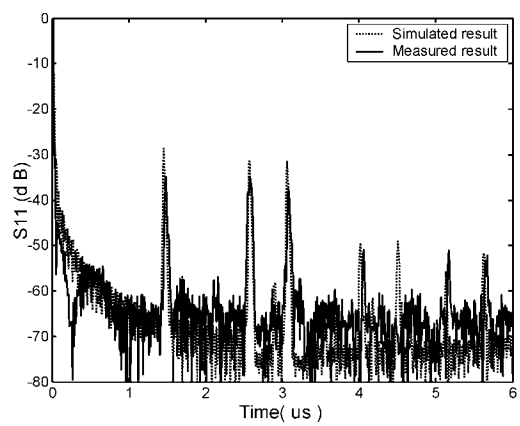

Fig. 7. (a) Measured S_{11} values and (b) simulated S_{11} values in time domain in case of no pressure.

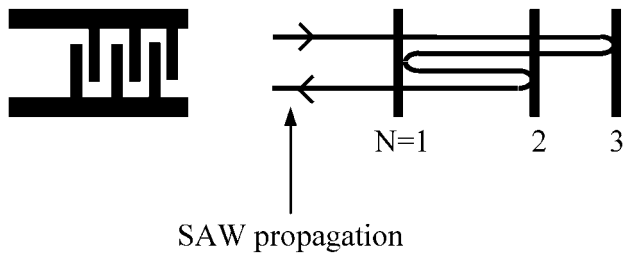

Fig. 8. Schematic of multiple reflections between bar-type reflectors.

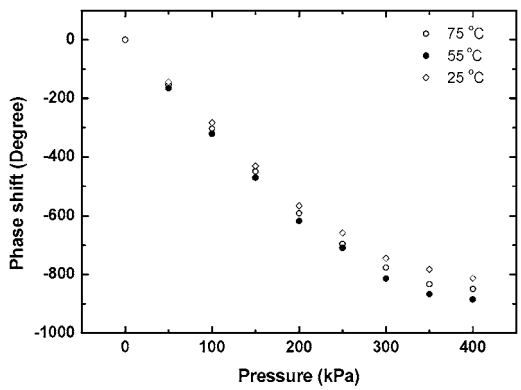

Fig. 9. Phase angle shifts of fabricated device depending on applied pressure and temperature variation.

noticeable deviation of the phase shifts was observed. From these results, we suggest that this SAW device is very promising for achieving a wirelessly requestable and batteryless human recognition sensor on an intelligent building floor.

6. Conclusion

We have presented a SAW pressure sensor composed of a reflective delay line and a bonding substrate underneath a diaphragm. Using the equivalent circuit model, the influence of the number of IDT finger pairs, acoustic aperture size, and reflector shape on the device properties was studied. Decreasing the number of IDT finger pairs improves the S/N ratio and sharpens the reflected peaks. The acoustic aperture affects the dynamic separation between the reflected peaks. Compared with an IDT-type reflector, a bar-type

reflector reduces the noise level owing to the decrease in self-reflection from the reflectors. FEM was used to calculate the bending of the diaphragm and the stress/strain distribution on the diaphragm. From the equivalent circuit model and FEM results, the optimal design parameters were determined, and a 440 MHz reflective delay line on a 41°YX $LiNbO_3$ substrate was developed. A high S/N ratio, sharp reflection peaks, and a large dynamic separation between the peaks were observed in reflection coefficient S_{11} measurements. A good agreement was observed between the simulated and measured results, suggesting that this equivalent circuit approach is a good selection for obtaining the optimal design parameters of the SAW pressure sensor.

References

1 L. Reindl: Int. Symp. Acoustic Wave Devices for Further Mobile Communication Systems 2004 (IEEE, Chiba University, 2004) p. 1.
2 L. Reindl, A. Pohl, G. Scholl and R. Weigel: IEEE Sensors Journal **1** (2001) 69.
3 G. Scholl, F. Schmidt, T. Ostertag, L. Reindl, H. Scherr and U. Wolff: Ultrasonics Symp. 1998 (IEEE, 1998) p. 595.
4 L. A. Francis, J. M. Friedt and P. Bertrand: Sens. Actuators, A **123** (2005) 360.
5 E. R. Benes, R. Groschl and F. Seifert: IEEE Transactions on Ultrasonics Ferroelectrics and Frequency Control **45** (1998) 1314.
6 L. Reindl, C. Ruppel, K. Riek, T. Pankratz and R. Weigel: Ultrasonics Symp. 1998 (IEEE, 1998) p. 355.
7 G. Schimetta, F. Dollinger, G. Scholl and R. Weigel: MTT-S Microwave Symp. 2001 (IEEE, Phoenix, 2001) p. 355.
8 D. A. Berlincourt, D. R. Curran and H. Jaffe: Physical Acoustics (Academic Press, New York, 1964) p. 169.
9 W. R. Smith: Circuit Model Analysis and Design of Interdigital Transducers for Surface Acoustic Wave Devices (Academic Press, New York, 1981) p. 99.
10 W. R. Smith, H. M. Gerad and J. H. Collins: IEEE Transaction on Microwaves Theory and Techniques **19 (**1969) 856.
11 C. Campbell: Surface Acoustic Wave Devices for Mobile and Wireless Communications (Academic Press, New York, 1998) Chap. 4.
12 K. Yamanouchi and K. Shibayama: J. Appl. Phys. **43** (1972) 856.
13 Y. Hiki: Annual Review of Materials Science **11** (1981) 51.
14 A. Talbi, O. Elmazria, F. Sarry and P. Alnot: Eurosensors XVI 2002 (Prague, 2002) p. 638.
15 H. Scherr, G. Scholl, F. Seifert and R. Weigel: Ultrasonics Symp. 1996 (IEEE, 1996) p. 347.